TU Delft

Delft University of Technology

Document Version
Final published version

Licence
CC BY-NC-ND

Citation (APA)
Yang, C., Abdelrahman, M., Khaloian-Sarnaghi, A., Dalal, Y., & van de Kuilen, J. W. (2026). Development and assessment of a nonlinear elasto–viscoelastic–viscoplastic model for cyclic and sustained loading with subsequent recovery in wood under compression. *Construction and Building Materials*, *545*, Article 148389. https://doi.org/10.1016/j.conbuildmat.2026.148389

Important note
To cite this publication, please use the final published version (if applicable).
Please check the document version above.

Copyright
In case the licence states “Dutch Copyright Act (Article 25fa)”, this publication was made available Green Open Access via the TU Delft Institutional Repository pursuant to Dutch Copyright Act (Article 25fa, the Taverne amendment). This provision does not affect copyright ownership.
Unless copyright is transferred by contract or statute, it remains with the copyright holder.

Sharing and reuse
Other than for strictly personal use, it is not permitted to download, forward or distribute the text or part of it, without the consent of the author(s) and/or copyright holder(s), unless the work is under an open content license such as Creative Commons.

Takedown policy
Please contact us and provide details if you believe this document breaches copyrights.
We will remove access to the work immediately and investigate your claim.

This work is downloaded from Delft University of Technology.

Construction and Building Materials 545 (2026) 148389

Contents lists available at ScienceDirect

Construction and Building Materials

journal homepage: www.elsevier.com/locate/conbuildmat

Development and assessment of a nonlinear elasto–viscoelastic–viscoplastic model for cyclic and sustained loading with subsequent recovery in wood under compression

Changxi Yang [a,*], Mostafa Abdelrahman [a,b], Ani Khaloian-Sarnaghi [c], Yaman Dalal [a], Jan-Willem van de Kuilen [a,d]

[a] Professorship of Wood Technology, Department of Materials Engineering, Technical University of Munich, Winzererstrasse 45, Munich, 80797, Germany
[b] Department of Civil Engineering, Suez Canal University, 4.5 Km the Ring Road, Ismailia, 8366004, Egypt
[c] Institute of Vehicle Safety, Graz University of Technology, Inffeldgasse 13, Graz, 8010, Austria
[d] Faculty of Civil Engineering and Geosciences, Biobased Structures and Materials, Delft University of Technology, Stevinweg 1, Delft, 2628, The Netherlands

ARTICLE INFO

Keywords:
Wood
Creep
Fatigue
Viscoelasticity
Viscoplasticity

ABSTRACT

Timber structures are evolving rapidly, featuring increasing spans, greater heights, longer service lives, and a broader range of applications. Some of these applications require a comprehensive understanding of wood's mechanical behavior, including both creep and fatigue. While wood is known to exhibit nonlinear time-dependent mechanical behavior, existing studies are largely limited to single or static loads, whereas complex load cases, such as varying stress levels or a mixture of fatigue and rheological effects, are underinvestigated.

To address this, this study presents an integrated experimental and modeling framework on European ash loaded in longitudinal compression under controlled constant climate conditions. The proposed program employed repeated load–recovery sequences on the same specimen, enabling comparison across multiple stress levels. Three types of loading were studied and compared—ramp, creep, and fatigue at two frequencies (0.1 Hz and 1 Hz). The results revealed elastic, viscoelastic, and viscoplastic strain components across all three loading types. Notably, the irrecoverable strain resulted from both the applied stress level and the duration of the load. Following these observations, a numerical model with a rate-dependent viscoelastic–viscoplastic framework was proposed and calibrated using multi-specimen creep data via a microstructure-based parameter-scaling approach. The calibrated model was used to predict fatigue test results at different frequencies and stress levels. While it captured the time-dependent strain response under sustained loading reasonably well, discrepancies of varying magnitudes were observed relative to the fatigue tests, indicating limitations of the current viscoplastic formulation in describing cyclic strain response. These findings offer new insights about the nonlinear creep and fatigue behavior of complex biomaterials such as wood, and provide opportunities to incorporate additional frequency-dependent mechanisms in advanced applications.

1. Introduction

Wood is a natural material composed of cellulose fibers embedded in a lignin–hemicellulose matrix [1]. The unique hierarchical structure of wood provides a relatively high strength-to-weight ratio; however, its inherent microstructure also poses challenges due to anisotropy, inhomogeneity, and heterogeneity. With the global pursuit of sustainable development goals, wood has been increasingly used as a structural material across a wide range of engineering fields, posing new challenges in material characterization and modeling. In applications such as road bridges, wind turbines, automotive and bicycle frames, and sports equipment (e.g., skis), the long-term, time-dependent mechanical response of wood becomes a crucial factor.

The study of wood loaded in compression parallel to the grain direction has long been a subject of research [2–6]. From a mechanical point of view, compression in wood is unique in that it typically displays greater nonlinearity than tension, primarily due to the early onset of kinks in cell walls [7–9]. Regarding modeling, two sources of nonlinearity exist in the compression of wood parallel to the grain: short-term plasticity and time-dependent viscoelasticity or viscoplasticity.

The plasticity theory has its roots in descriptions of metal deformation [10–12], originally developed to capture the strain occurring

* Corresponding author.
E-mail address: changxi.yang@tum.de (C. Yang).

https://doi.org/10.1016/j.conbuildmat.2026.148389
Received 11 July 2026; Received in revised form 2 September 2026; Accepted 27 September 2026
Available online 7 October 2026
0950-0618/© 2026 The Authors. Published by Elsevier Ltd. This is an open access article under the CC BY-NC-ND license (http://creativecommons.org/licenses/by-nc-nd/4.0/).
Open access funding enabled and organized by Projekt DEAL.

beyond the proportional limit in short-term strength tests. In this context, plastic strain is assumed to take place instantaneously once the applied stress exceeds a certain threshold. It represents an idealized, rate-independent, irrecoverable strain. In contrast, viscoelasticity theory [13,14] originates from descriptions of rate-dependent strain that develops gradually under sustained stressing or straining, which is recoverable after a finite or, in some cases, indefinitely long period upon load release.

One of the earliest insights into the short-term nonlinearity of wood was provided by Robinson [15], who attributed the permanent deformation to the formation of kinks — originally referred to as "slip-planes" — that precede fiber buckling and failure. Following this, several researchers have attempted to correlate the onset of kinks with a specific level and duration of applied stress. Kisser and Steininger [16] investigated three softwood species and found that the first microscopic kinks formed consistently at around 50% of the ultimate bending strength during 2-hour bending tests. For compression parallel-to-grain, Norway spruce was found to form kinks as early as 25% of the ultimate strength, while the amount of kinks increased considerably at a stress level of 50% to 65% [17], with load duration as short as one minute. Whether these microstructural changes can be directly associated with the onset of macroscopic material nonlinearity remains unclear, particularly given the relatively low stress levels reported.

In contrast to microscopic kink investigations, the proportional limit in stress–strain curves observed from short-term strength tests provides a direct indication of short-term nonlinearity. The proportional limit marks the transition point up to which the stress–strain relationship remains approximately linear. For compression parallel-to-grain in wood, the proportional limit is generally considered higher than that in bending [18]. The work by Bolza and Kloot [19] provided a comprehensive summary of various mechanical properties for 174 Australian wood species. The reported data showed a significant variability of the proportional limit on wood species. For instance, white beech exhibited a proportional limit of 77% under compression parallel to the grain. In comparison, silvertop ash exhibited nonlinear strain development at already 62% of the ultimate compressive strength. However, a more recent study conducted across multiple German research institutes [20] suggested considerably higher proportional limit values. Although results varied slightly from institute to institute for beech and birch harvested from the same forestry stand, both species exhibited proportional limits in the range of 85% to 90% under longitudinal compression. Similar thresholds between 80% and 85% were reported in [21] for white spruce, although the samples were conditioned to moisture contents of 9% and 18%, which differs from the 12% in the previously-mentioned studies [19,20].

It has been well established that wood exhibits nonlinear viscoelasticity under sustained loading [21–24]. Only when the stress level, temperature, and moisture content remain relatively low can it be considered as linear viscoelastic [25]. For sustained loading, the onset of nonlinear viscoelastic behavior can also be identified by analyzing the relationship between creep strain and applied stress. Since creep strain evolves with time, the comparison must be performed at a fixed load duration. To date, investigations on this topic remain insufficient. A study on hoop pine under uniaxial longitudinal compression showed a nonlinearity threshold of 70% for a load duration up to 60 h [18]. Another study with a series of 24-hour compression tests on white spruce conditioned to 9% and 18% moisture content reported nonlinearity thresholds of approximately 80% and 60% of the corresponding conditioned short-term strength, respectively [21]. More recently, Kuwamura [26] reported a nonlinearity threshold exceeding 50% for Japanese cedar, spruce, pine, and fir subjected to longitudinal compression. The specimens were wrapped in plastic film to minimize moisture exchange, and creep was monitored over 10 h.

Besides determining nonlinearity thresholds, researches have been carried out to characterize the different strain components associated with viscoelasticity [21,24,27,28]. Most of these studies employed creep-recovery tests at constant stresses and specific load durations to partition the total strain. Upon unloading, the time-dependent recoverable portion is classified as viscoelastic, while residual strain, remaining after a specified recovery period is considered permanent and is commonly referred to as "viscous" in the literature [24]. However, the term "viscous" typically refers to dashpot-like flow behavior, which occurs without a stress threshold. In reality, the non-recoverable strain observed after unloading may arise from plastic or viscoplastic deformation. To avoid ambiguity, the term "inelastic" will be used throughout the following descriptions instead of "viscous" to denote the residual strain remaining at the end of recovery.

Investigations into strain component partitioning in wood can be broadly categorized into two approaches: the first characterizes the different strain components in relation to stress levels, with the observation time fixed; whereas the second approach focuses on the evolution of various strain components with respect to load duration, where the stress level is fixed.

For the first approach, an example of compression parallel to grain can be found in [21]. A wide range of stress levels from 40% to 80% was covered, and the strain was recorded for 24-hour creep loading and subsequent recovery of the same duration. For the group tested at a constant 18% moisture content, both viscoelastic and inelastic strain components were observed to accumulate nonlinearly with increasing stress levels. Furthermore, inelastic strain was already detectable at a stress level as low as 20%.

For the second approach, Bach [29] performed pulsating compression tests on matched samples at relatively high stress levels of above 70%. Since the applied square-wave pulsating load had frequencies below 0.1 Hz, it can be considered as comparable to creep loading [30]. The matched samples were loaded for a specific fraction of their assumed fatigue life, followed by a recovery test lasting longer than three times the fatigue load duration. A constant climate condition of 75% relative humidity was adopted. The results suggested a more pronounced accumulation of the inelastic strain close to failure. However, a detailed relation among all three strain components was not clearly illustrated.

So far, the short-term and time-dependent nonlinearities of wood have been treated as distinct phenomena in modeling [31,32]. Nonlinearity observed in short-term tests is typically attributed to rate-independent plasticity, whereas nonlinearity from longer-duration creep tests is modeled as a result of viscoelasticity. However, short-term loading used to characterize plasticity is still applied over a measurable time span. Most standards regulate the loading rate to ensure specimen failure within a few minutes, typically two to seven minutes [9,30]. Nonlinear strain observed in short-term strength tests is not necessarily purely plastic, but may also include time-dependent contributions that manifest during the loading phase.

Viscoplasticity theory generalizes plasticity by defining an inelastic strain rate that depends on stress (and other internal variables). A widely used theory is the Perzyna-type overstress model originating from [33]. Although developed in the context of metallic materials, it applies to a wide range of materials such as rubber, geomaterials, concrete, and composites [34]. A key feature of the Perzyna-type viscoplastic model is its time-dependent inelastic flow, which means the inelastic strain requires time to develop after the applied stress exceeds the yield threshold. To the authors' knowledge, investigations into the viscoplastic characterization of wood under compression remain scarce. Nevertheless, the history effect reported in repeated compression fatigue loading blocks [35] is most likely attributable to viscoplastic strain accumulation.

This study develops and demonstrates an experimental and numerical modeling framework for characterizing the nonlinear time-dependent compression behavior of wood. Using small, straight-fiber solid-wood specimens, this study examines the elastic, delayed-elastic, and stress-dependent inelastic responses of European Ash under strictly controlled temperature and moisture conditions (20°C, 65% relative



Fig. 1. European ash compressive specimens: from preparation to test.

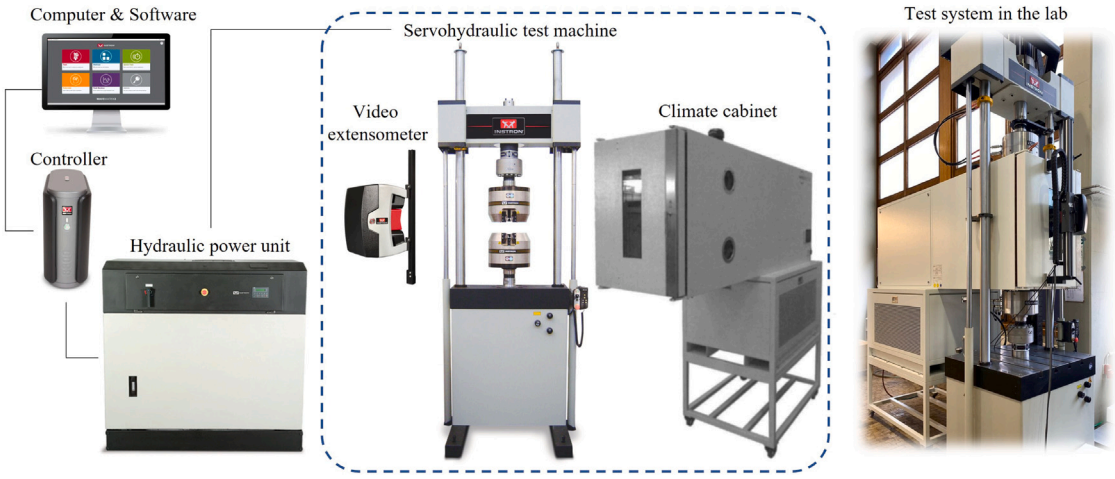


Fig. 2. Servohydraulic test system with video extensometer and climate cabinet.

humidity). Wood exhibits pronounced anisotropy in the longitudinal, radial, and tangential directions. To enable a focused, accurate characterization of its nonlinear response, a single loading orientation, parallel to the grain, is investigated. Specimen-to-specimen scatter originated from anatomical variability and heterogeneity is unavoidable for natural materials like wood. This has been traditionally addressed through careful selection of specimens that are assumed to have similar mechanical properties [26,29,36]. More recently, probabilistic approaches have also been implemented to capture the inherent material variability of wood and bamboo products in creep [37]. In this work, we adopt a different approach: the influence of specimen-to-specimen variability is partially migrated through an experimental design employing stepwise-increasing stress histories, allowing the response at multiple stress levels to be investigated within the same specimen. Additionally, the repeated load-recovery sequences are employed over a range of loading rates and durations, covering ramp loading, short-period creep, and short-period fatigue.

Subsequently, a coupled elasto–viscoelastic–viscoplastic numerical model is developed and calibrated using the obtained multi-specimen dataset. Since a single test does not contain sufficient information to identify time-dependent material parameters, a MoE-based calibration framework is developed to account for specimen-to-specimen variability while facilitating the use of a common set of material parameters for all test specimens. The proposed calibration framework has its roots in the hierarchical structure of wood and incorporates microstructural variability via a homogenized scaling parameter. Using the proposed methodology, the model is calibrated using creep test data. The identified parameters are further implemented, without further calibration, to predict the strain response under different fatigue loading conditions. Analysis of the discovered discrepancies between prediction and fatigue tests helps to identify additional mechanisms that may be required to fully describe the cyclic response. By employing a unified framework and comparing the results for loading conditions that are conventionally treated independently, this study establishes a basis for further constitutive model development. Moreover, the proposed parameter-scaling framework enables physically meaningful calibration, providing a basis for understanding the nonlinear, time-dependent mechanical behavior of highly hierarchical and structurally complex biological materials.

2. Experimental design

2.1. Materials and experimental setup

The preparation process of test specimens is shown in Fig. 1. The samples investigated in this study were knot-free specimens from European ash (*Fraxinus excelsior*), with dimensions of 25 mm × 25 mm ×75 mm. Mechanical behavior of the material under compression parallel to the fiber directions was investigated. Therefore, the specimens were cut with fibers as straight and parallel to the longitudinal direction as possible. Before testing , all specimens were conditioned in a climate-controlled room for at least three months. The average density of the specimens, determined at 20° and 65% relative humidity, reaches 500 ± 5 kg/m^3.

As illustrated in Fig. 2, all tests were conducted using an 8802 Instron servohydraulic machine equipped with a 250 kN load cell. The grip area is enclosed by a Weiss Technik climate cabinet to ensure a controlled climate during testing. The average longitudinal strain was recorded over a gauge length of 50 mm, through a non-contact video extensometer (AVE 2) mounted on the glass door of the cabinet. No friction-reducing interlayers were used between the steel compression plate and the specimen. Therefore, the risk of having end-friction

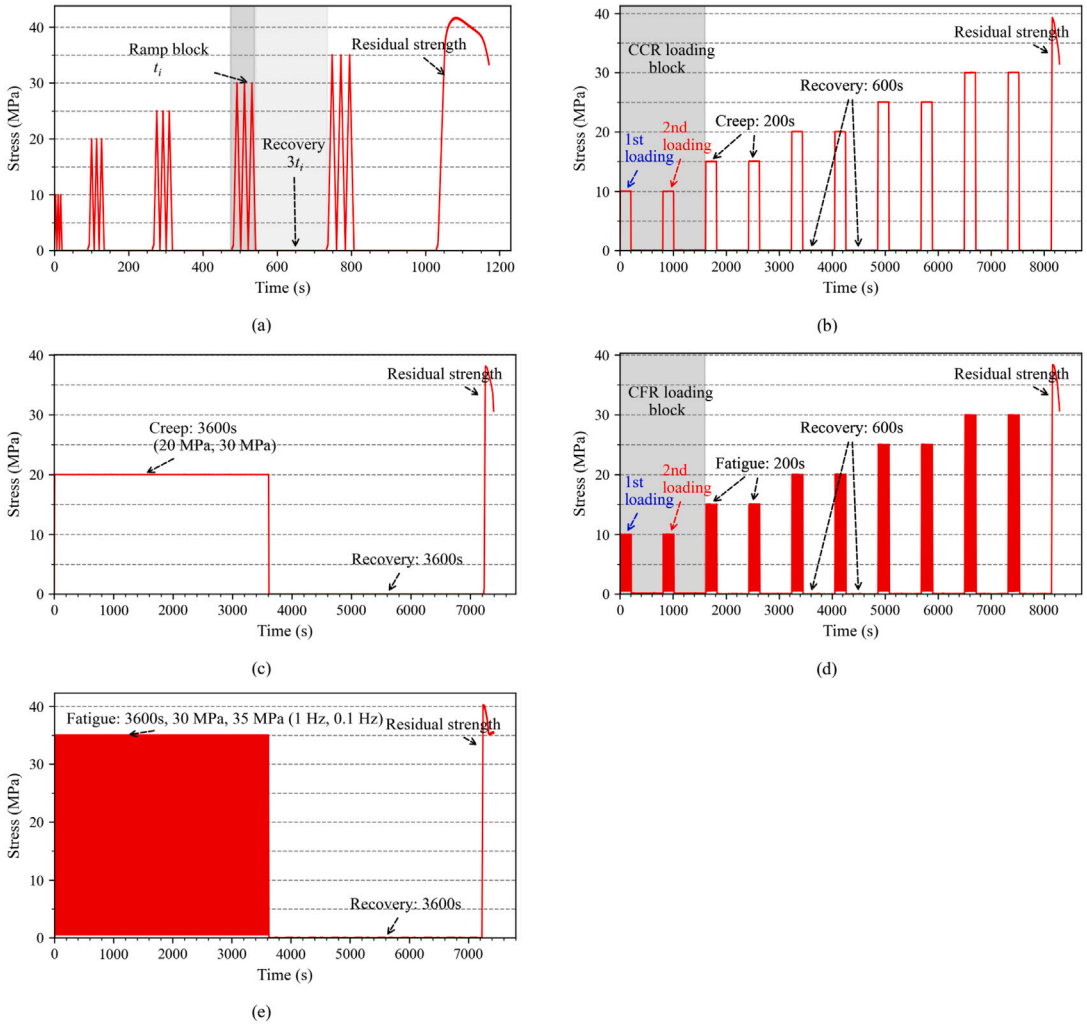


Fig. 3. Experiment: (a) Cyclic ramp-recovery (CRR) tests; (b) Cyclic creep-recovery (CCR) tests; (c) Creep-recovery (CR) tests; (d) Cyclic fatigue-recovery tests, consisting of two frequencies: 0.1 Hz (CFR01) and 1.0 Hz (CFR1); (e) Fatigue-recovery tests, consisting of two frequencies: 0.1 Hz (FR01) and 1.0 Hz (FR1).

effects and non-uniform stress states near specimen ends is not entirely absent. Nevertheless, longitudinal strain was measured over the central section of the specimen, thereby reducing the direct influence of the platen–specimen interfaces.

To determine the required stress level, the short-term compressive strength of five randomly chosen specimens was measured using static tests at a displacement rate of 1.5 mm/min. The strength obtained from the five specimens was 40.1 ± 2.4 MPa.

2.2. Experimental procedure

The proposed protocol comprises three loading types: ramp, creep, and fatigue. For each loading type, the influence of stress level is investigated by applying loading–recovery sequences at multiple levels — both below and above the proportional limit — to identify the onset of nonlinearity. Multiple stress levels are applied to the same specimen, with recovery phases between sequences to reduce the effects of prior loading history. For both creep loading and fatigue loading, relatively short loading intervals are employed to enable accelerated material characterization while maintaining comparability with the previous study [35]. The experimental program also includes longer loading durations of approximately one hour, enabling a broader assessment of the evolution of time-dependent strain components.

Because the aim was to apply and to compare multiple stress levels on the same test specimen, several test groups incorporated stepwise increases in stress, as shown in Fig. 3. Considering that the average strength value of the investigated material reached approximately 40 MPa, the stress interval was set to 5 MPa. Since the intention was not to cause direct failure, the highest stress applied for any creep loading was set to 30 MPa, corresponding to 75% of the ultimate strength. For the cyclic ramp-recovery test or short-duration fatigue test, the applied stress was no more than 35 MPa.

A static test with a displacement rate of 1.5 mm/min was conducted at the end of all tests to determine the residual strength (f_r) of the material. Under the assumption that there is limited internal damage development during the relatively short loading sequences, the residual strength can be considered indicative of the original strength of the tested specimen.

To ensure repeatability, two replicates were tested at each new test group. When a test group represented only an extension of a previous group with respect to loading duration, only one additional test was performed. The resulting data were then compared with those of the corresponding previous group to assess consistency. We note that the narrow density range of our specific material enabled us to draw some conclusions about the nonlinearity threshold for the focused dataset and served only as a proof of concept for the proposed constitutive framework. The identified parameters, however, should not be considered representative for low-density European ash in general. A large number of specimens that capture the statistical variability of wood need to be evaluated to provide a general characterization of its time-dependent behavior.

Table 1
Density of specimens for each test group.

Test group	Density (kg/m^3)	
	Specimen 1	Specimen 2
CRR (Cyclic ramp recovery)	500	510
CCR (Cyclic creep recovery)	505	505
CR20 (Creep recovery, 20 MPa)	500	–
CR30 (Creep recovery, 30 MPa)	495	–
CFR01 (Cyclic fatigue recovery, 0.1 Hz)	500	505
CFR1 (Cyclic fatigue recovery, 1 Hz)	495	505
FR0130 (Fatigue recovery, 0.1 Hz, 30 MPa)	505	–
FR0135 (Fatigue recovery, 0.1 Hz, 35 MPa)	500	–
FR130 (Fatigue recovery, 1 Hz, 30 MPa)	500	–
FR135 (Fatigue recovery, 1 Hz, 35 MPa)	500	–

For test groups with stepwise increases in stress, a recovery phase lasting three times the duration of preceding loading was adopted to separate the dominant viscoelastic deformation from unrecovered deformation. It should be noted that the current selection does not imply complete viscoelastic recovery, as wood is known to exhibit delayed viscoelastic recovery under constant climate conditions. Therefore, the identified decomposition between viscoelastic and viscoplastic strain should only be interpreted within the experimentally investigated time scale and the corresponding climate conditions.

A detailed description of the five test schemes applied in this work is provided in the following sections. The density values of all tested specimens, together with their test groups, are listed in Table 1.

2.2.1. Cyclic ramp-recovery test

In the first stage, the nonlinear properties of the material were investigated through cyclic ramp-recovery (CRR) tests. As illustrated in Fig. 3(a), the CRR test consisted of ramp blocks with stepwise increasing stress level (SL). Each ramp block contained three consecutive loading–unloading phases at the same stress level, with a constant ramp rate of 3 MPa/s. This repetition helps to identify any viscoelastic or viscoplastic strains, since rate-independent elastic or plastic strain theoretically does not lead to differences in the accumulated strain among repeated loading sequences. Elastic strain is expected to remain consistent during each loading, and fully recover during unloading. In contrast, rate-independent plastic strain develops entirely during the first loading sequence and remains unchanged during unloading. In either case, subsequent loading–unloading phases should follow the same strain trajectory as the previous ones.

A recovery phase, lasting three times the duration of the ramp load block, was implemented after each block to quantify the accumulated inelastic strain, as depicted in Fig. 3(a). Herein, only linear viscoelasticity and viscoplasticity are taken into consideration. It is assumed that the recovered strain highlights any viscoelastic components developed during the very short-term ramp loading (approximately 15 s). The remaining permanent strain, on the other hand, can be used to distinguish the viscoplastic strain component.

2.2.2. Cyclic creep-recovery test

The effect of short-term viscosity was further examined through cyclic creep-recovery tests (“CCR”), as depicted in Fig. 3(b). The same ramp rate as CRR tests was applied for loading and unloading. However, each SL was held constant for 200 s to investigate the accumulation of creep strain. After unloading, a recovery phase of 600 s was implemented, which is assumed to be long enough to distinguish the dominant irrecoverable strain from recoverable viscoelastic strain. Similar to CRR tests, each creep-recovery block in the CCR tests was repeated twice for the same SL on the same specimen. If for the same SL, the second block showed a different strain trajectory from the first block, nonlinearity can be identified. Herein, the focus is laid on the accumulation of strain during the sustained loading phase. At the end of the test, a residual strength test was conducted on each specimen to determine the residual strength.

2.2.3. Creep-recovery test

After obtaining the strain accumulation results from CCR tests, two stress levels were selected for implementation in extended creep-recovery (“CR”) tests—one below the potential inelastic threshold and the other above. As depicted in Fig. 3(c), the CR test consisted of a one-hour creep test, a one-hour recovery, and a subsequent residual strength test. The goal is twofold: first, the CR test result can be directly compared to the corresponding creep intervals with the same SL in CCR tests. If the total strain accumulation within the first 200 s approximately overlaps, the previous CCR results are verified, indicating that the effect of prior lower-SL loading can be considered negligible for the subsequent intervals. Second, by extending the creep loading to one-hour loading, the evolution of strain components for longer time scales can be qualitatively examined. Only one specimen was tested for each target SL, as the previous CCR test already contained two replicates with a partially overlapping testing procedure.

2.2.4. Cyclic fatigue-recovery test

The short-period cyclic fatigue-recovery tests (“CFR”) were conducted in a similar way to CCR tests, which is shown in Fig. 3(d). For fatigue tests under compression, the complete release of load during cyclic loading can trigger mechanical instability in the servohydraulic testing system. To prevent this, the minimum stress in each loading cycle was set to a fixed value of 0.5 MPa. To include the frequency effect, two test groups were designed, with loading frequencies of 0.1 Hz and 1 Hz, respectively. The lower frequency of 0.1 Hz is considered comparable to a short “static” load in terms of damage accumulation, as suggested in [29,30]. Each loading block consisted of two identical loading-recovery intervals, with a loading duration of 200 s per interval. This corresponded to 20 cycles at 0.1 Hz and 200 cycles at 1 Hz. The objective is to validate whether the strain components observed in creep tests can also be identified under fatigue loading of the same total duration, and whether they exhibit similar trends across different loading frequencies.

2.2.5. Fatigue-recovery test

Similarly, fatigue-recovery tests (“FR”) were conducted according to Fig. 3(e). For the FR tests, only the highest SL (30 MPa) reached during CFR tests was implemented, together with an additional group at 35 MPa. This is because fatigue loading was expected to result in less strain accumulation than creep loading of the same total duration at the same stress level. Using a low SL may not result in measurable strain accumulation within the short timeframe of the fatigue test. Two test frequencies were included, each requiring only one test specimen. The fatigue loading lasted for one hour, equivalent to 360 cycles and 3600 cycles at 0.1 Hz and 1 Hz, respectively.

2.3. Data analysis

Two major analyses were performed on the test data obtained: strain analysis and proportional limit analysis. The strain analysis focused on decomposition of elastic, viscoelastic and inelastic strain components and their relationship with loading time and stress levels. Whereas the proportional limit analysis helped to identify nonlinearity thresholds during residual strength tests under different loading cases.

To facilitate the strain analysis, the following hypotheses are made:

- In the CRR, CCR, and CFR tests, each loading period was followed by a recovery period that lasted three times the duration of loading. This is considered sufficient to recover the majority of viscoelastic strain. The identified unrecovered strain should not be considered as ‘true’ viscoplastic flow representative of the general material behavior, but rather as a viscoplastic constitutive component that describes the material response within the investigated time scale. In reality, the residual strain at the end of the recovery may continue to recover over a much longer time span, especially when subjected to moisture changes [38,39].

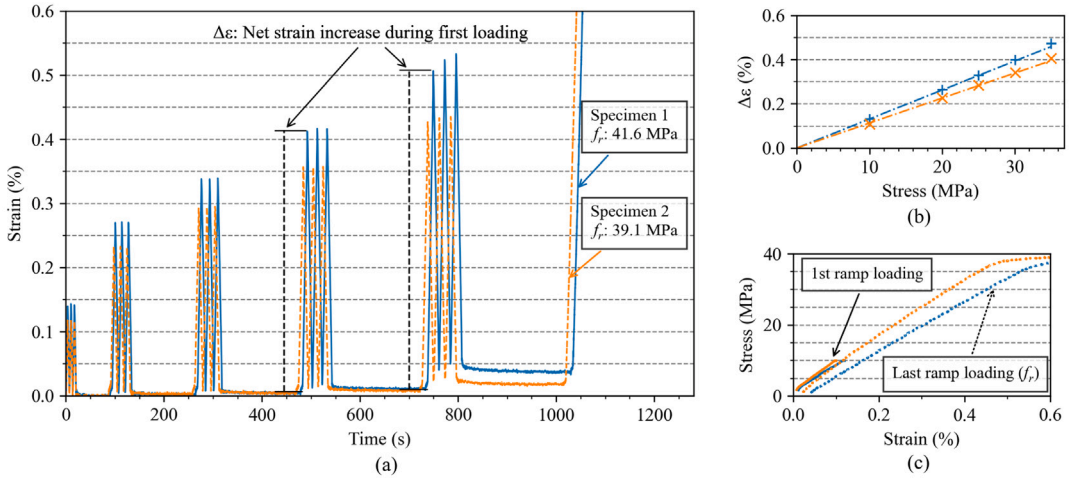


Fig. 4. Results of cyclic ramp-recovery (CRR) tests. The definition of net strain increase $\Delta\varepsilon$ is demonstrated in subfigure (a) using Specimen 1 as an example.

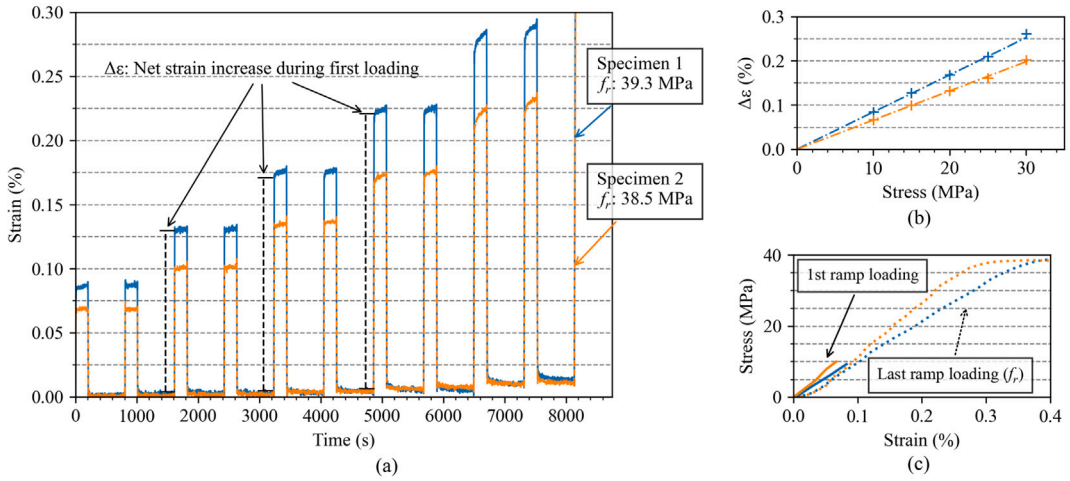


Fig. 5. Results of cyclic creep-recovery (CCR) tests. The definition of net strain increase $\Delta\varepsilon$ is demonstrated in subfigure (a) using Specimen 1 as an example.

- Although a slight recovery of viscoelastic strain may occur during unloading, it is assumed that the majority of recovery only starts after the load is fully released.
- Given the relatively low applied stress and the short loading duration — for cyclic creep and cyclic fatigue tests, the SL is set to maximum 75% of the ultimate strength, and each loading interval lasts for only 200 s — we assumed that any micro-damage developed during these loadings is insufficient to cause any reduction in residual strengths. Consequently, the residual strength measured at the end of the test is considered to reflect the magnitude of the specimen's initial strength.

3. Experimental results and discussion

3.1. Strain analysis

3.1.1. Cyclic ramp-recovery test (CRR)

The resultant strain measured for both specimens during CRR tests is plotted in Fig. 4(a). Specimens are color-coded, with their residual strengths annotated directly beside each strain–time curve. Fig. 4(b) plots the net strain increase during the first loading step of each ramp block against the applied stress. The stress–strain curves from the first ramp loading block and from the residual strength loading (the last ramp) are illustrated in Fig. 4(c).

The residual strengths depicted in Fig. 4(a) differ by 6% between the two specimens. Whereas the modulus of elasticity calculated from Fig. 4(b) shows a comparably greater difference, 7.5 GPa for specimen 1 versus 8.5 GPa for specimen 2. This variation reinforces that, even under carefully controlled density conditions, the strain response across different European ash specimens may vary considerably.

From Fig. 4(b), it can also be observed that for both specimens, a linear trend persists up to approximately 30 MPa. At 35 MPa, the observed net strain increase indicates additional strain accumulation beyond linear elastic behavior. This is also consistent with the observation shown in Fig. 4(c), where the potential onset of inelastic deformation occurs after reaching 30 MPa.

For each SL, three consecutive loading–unloading sequences are performed without any recovery phases. Therefore, any viscoelastic strain developed from the previous loading sequence cannot be recovered, and a reduced magnitude of viscoelastic strain develops again in the second and third sequences, leading to additional strain accumulation in the subsequent loading. If the applied SL exceeds the viscoplastic yield threshold, a similar accumulation effect can be observed across the consecutive loading–unloading sequences.

Fig. 4(a) indicates that, overall, the viscoelastic or viscoplastic accumulation effect is not entirely absent, but appears to be very limited up to the fourth block (30 MPa), which corresponds to approximately 75% of the mean ultimate strength. At 30 MPa, the accumulated strain of three consecutive loading sequences shows a slight increase in

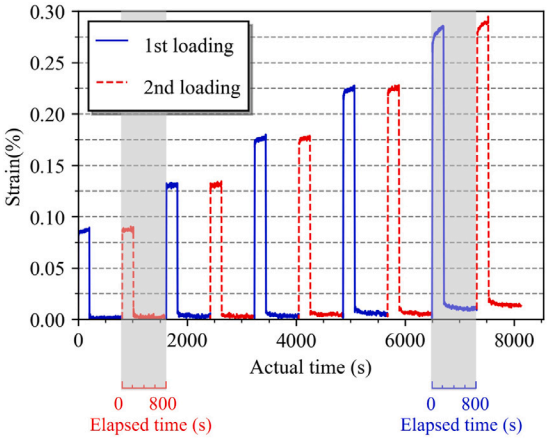


Fig. 6. Illustration of "Elapsed time" using CCR tests as an example.

specimen 1, whereas this change is less pronounced in specimen 2. At 35 MPa, both specimens exhibit a clear increase in accumulated strain across the three consecutive loading sequences.

For both specimens, the presence of unrecovered strain becomes more evident at 30 MPa and increases significantly at 35 MPa. In contrast, the recovered strain remains relatively low across the entire stress range (10–35 MPa) but also increases with stress. This implies a more pronounced effect of viscoplasticity than of viscoelasticity at stresses above 30 MPa. Therefore, the nonlinearity threshold in the CRR tests can be estimated to lie between 30 and 35 MPa, corresponding to approximately 75%–88% of the ultimate strength.

In Fig. 4(c), it is clear that, due to accumulated unrecovered strains, a noticeable shift of the curves to the right is observed for both specimens. However, no significant difference is observed between the slopes of the first and last loadings, indicating the absence of a softening effect under the given test conditions. This confirms our previous assumption that very little to negligible damage is present during the conducted tests.

3.1.2. Cyclic creep-recovery test (CCR)

The total strain accumulation and recovery from CCR tests is illustrated in Fig. 5(a). Each block comprises two identical loading-hold-recovery intervals at the same SL. The stress is held for 200 s, allowing greater development of viscoelasticity or viscoplasticity than in CRR tests. To avoid excessive damage development, a slightly modified stress map is applied—the highest SL reached in this setup is only 30 MPa instead of 35 MPa.

If the applied SL is sufficiently low to produce only viscoelastic strain and avoid triggering any additional irrecoverable strain, the second loading step at the same SL should replicate the strain accumulation and recovery trajectory observed in the first loading step, as the viscoelastic strain is assumed to recover entirely during the first recovery.

To better visualize this behavior, the concept of "elapsed time" is introduced, as illustrated in Fig. 6. For each loading–hold–recovery interval, the strain–time curve is shifted to the origin so that the individual responses can be directly overlaid. Because each stress level (SL) contains two identical loading intervals, they are color-coded for clarity: the first loading step is shown in blue, and the second loading step in red.

The shifted strain–time curves are shown in Fig. 7, where the strain response of the same specimen is plotted against the elapsed time within each interval. It can be observed that for specimen 1, there is a negligible difference between the first and second loadings up to 25 MPa. For specimen 2, this difference, although very small, is already visible at 20–25 MPa.

Given that both specimens had similar residual strength — 39.3 MPa and 38.5 MPa, respectively — the average threshold for nonlinearity in the CCR tests can be estimated to be approximately between 20 MPa and 25 MPa, corresponding to 50%–63% of the ultimate strength. Compared to the previous 75%–88% obtained in CRR tests, the nonlinearity threshold is much lower. This implies that the longer load duration in CCR tests potentially decreases the nonlinearity threshold compared to CRR tests.

According to Fig. 5(b), the elastic strain developed during the initial loading phase within each block demonstrates strong linearity. However, despite the similar residual strength values observed in both specimens, their respective moduli of elasticity show a considerable difference—11.7 and 14.9 GPa, respectively, for specimen 1 and specimen 2.

Similar to the CRR tests, the stress–strain curves from the first and the last ramp loading do not exhibit an apparent reduction in slopes, as shown in Fig. 5(c). The two stress–strain curves of the same color show trajectories that are roughly parallel.

3.1.3. Creep recovery test (CR)

Two stress levels — 20 MPa and 30 MPa — are selected for extended creep-recovery (CR) tests.

The accumulated strain is normalized with respect to the initial elastic strain and presented in Fig. 8, alongside strain recordings from previous CCR tests conducted at the same stress. The residual strengths for specimens tested at 20 MPa and 30 MPa are 38.2 MPa and 38.8 MPa, respectively. It can be observed from Fig. 8 that, after normalization, the strain accumulation curves from creep tests conducted over different time scales align closely for the same stress level.

Furthermore, the strain–time curves of one-hour testing at 20 MPa and 30 MPa follow significantly different trajectories. The one at the lower SL exhibits a nearly asymptotic behavior at the end of the test, whereas the curve at the higher SL does not. A closer look at the recovery phase suggests that this difference in accumulated strain is more likely driven by viscoplastic effects than by viscoelasticity. This conclusion arises from the observation that the recovered strain in the higher-stress-level test does not differ substantially from that of the lower-stress-level test, while the unrecovered strain shows a pronounced increase with stress level.

Another interesting point can be found in the group that is tested at 20 MPa. After a loading duration of 200 s, the accumulated strain almost fully recovers. This corresponds to the previous observation that the stress threshold for clear viscoplastic strain accumulation within a 200-second loading period is evaluated to be between 25 MPa and 30 MPa. However, the specimen subjected to the one-hour loading period exhibits a noticeable amount of unrecovered strain at the end of the recovery phase. This confirms that the apparent "viscoplastic threshold" may decrease with increasing loading duration. In fact, this observation can be well explained by the duration-of-load theory. If the amount of viscoplastic strain development is considered to reflect the extent of microscopic damage accumulation (fiber buckling in this case), then a longer load duration should indeed induce more damage accumulation at the same stress level.

3.1.4. Cyclic fatigue-recovery test (CFR)

Two test frequencies, 0.1 Hz and 1 Hz, are adopted in CFR tests. The total strain evolution, along with the change in modulus of elasticity, is illustrated in Figs. 9 and 10, respectively. Each block comprises two identical loading-fatigue-recovery intervals at the same SL, similar to the previous CCR tests.

From Figs. 9(a) and 10(a), it can be observed that, at both test frequencies, the strain accumulation due to viscoelasticity and/or viscoplasticity begins at a much higher SL than in CCR tests. For all four specimens tested, visible viscoelastic strain accumulation begins at 30 MPa, but only to a very limited extent. For most of the applied stress levels, the unrecovered strain at the end of the recovery phase is

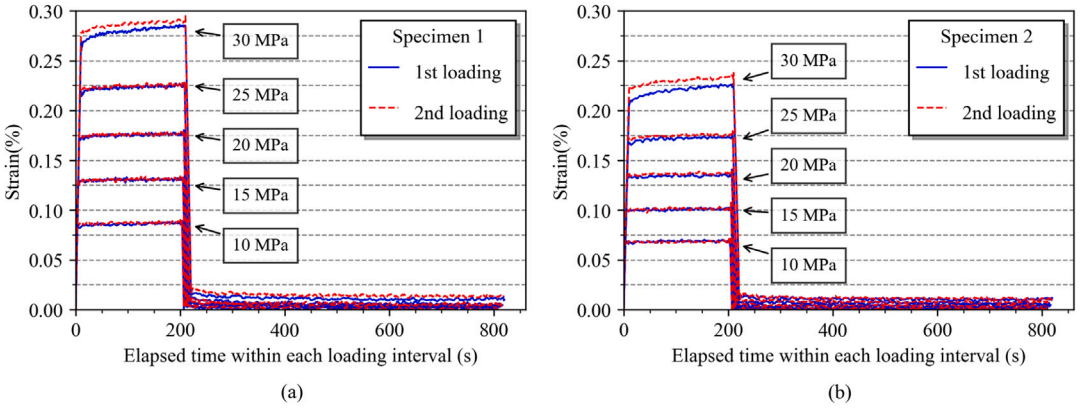


Fig. 7. History effect of cyclic creep-recovery (CCR) tests.

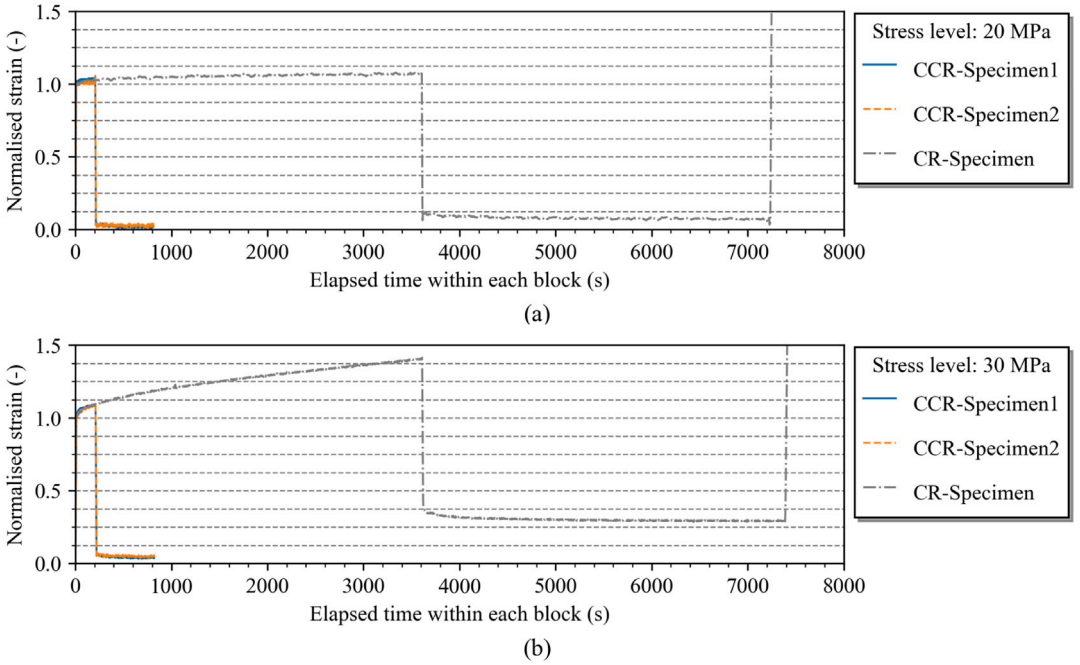


Fig. 8. Comparison between creep-recovery (CR) and cyclic creep-recovery (CCR) tests at the same stress level.

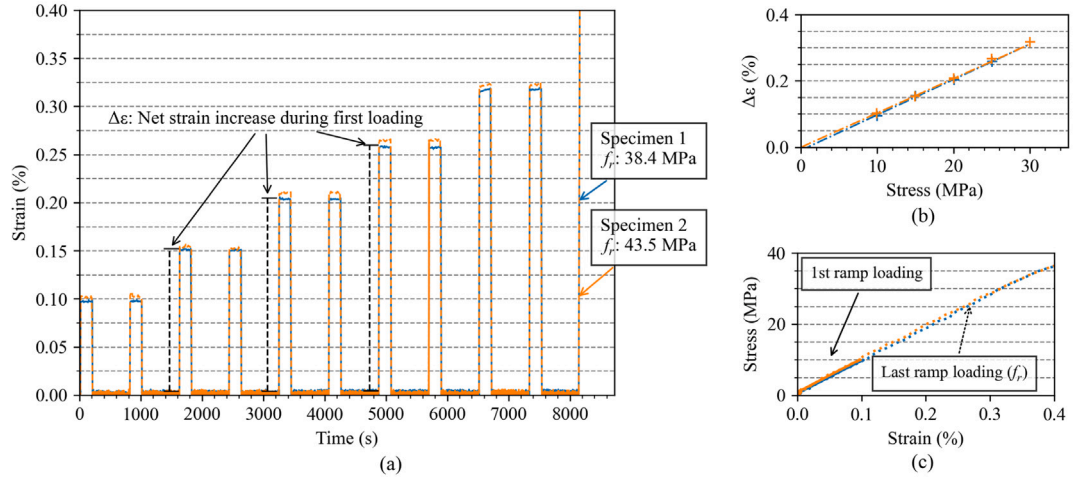


Fig. 9. Results of cyclic fatigue-recovery tests at test frequency of 0.1 Hz (CFR01). The definition of net strain increase $\Delta\epsilon$ is demonstrated in subfigure (a) using Specimen 1 as an example.

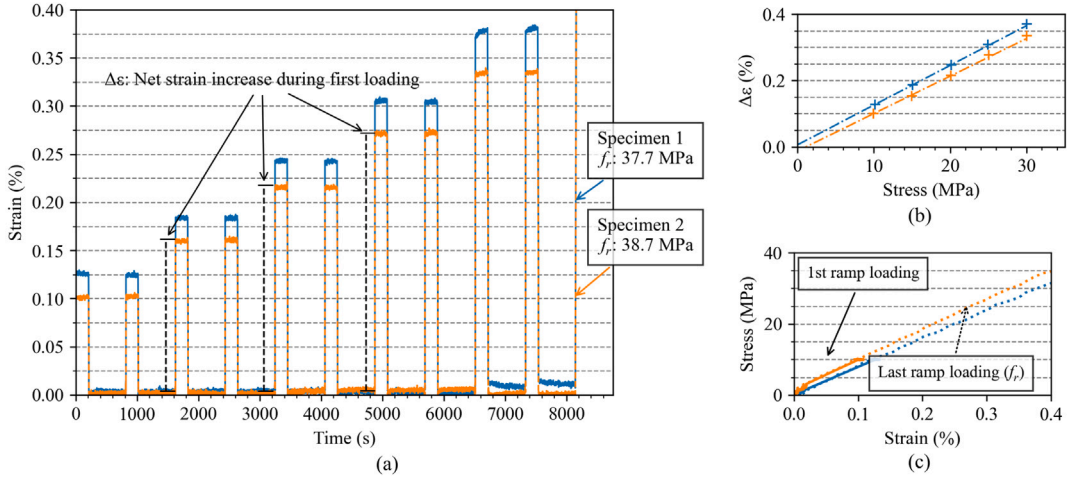


Fig. 10. Results of cyclic fatigue-recovery tests at test frequency of 1.0 Hz (CFR1).

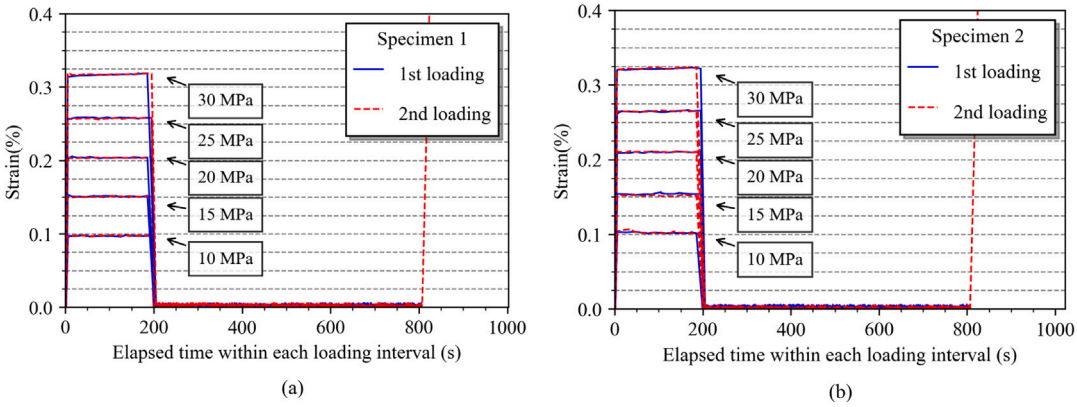


Fig. 11. History effect of cyclic fatigue-recovery tests at test frequency of 0.1 Hz (CFR01).

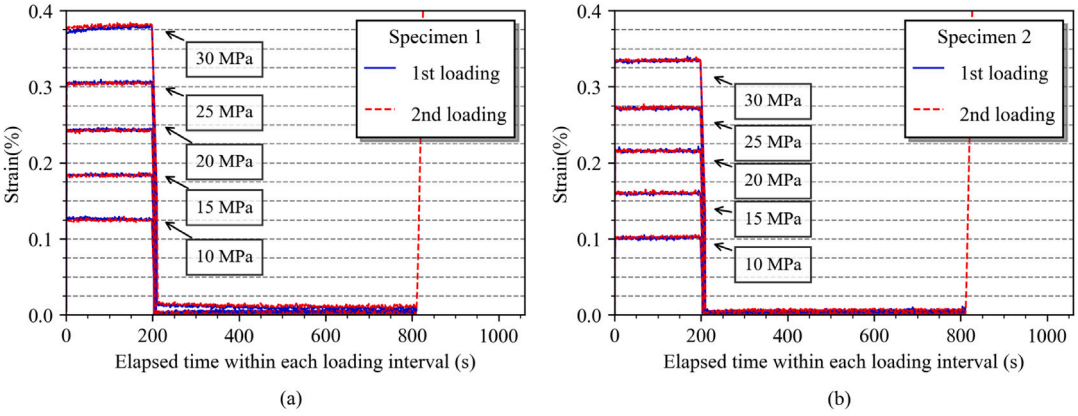


Fig. 12. History effect of cyclic fatigue-recovery tests at test frequency of 1.0 Hz (CFR1).

negligible at both test frequencies. Only the specimen with relatively low residual strength (37.7 MPa, tested at 1.0 Hz) exhibits distinct residual strain during recovery after being loaded to 30 MPa.

The net strain increase depicted in Figs. 9(b) and 10(b) shows clear linearity in the stress range 0–30 MPa, similar to the CRR and CCR tests. Since a very limited amount of viscoplastic strain develops in the conducted fatigue tests, the shift of the stress–strain curves from the first to the last ramp loading in Figs. 9(c) and 10(c) is also negligible. Also, there is no visible softening effect based on the slope of the stress–strain curves shown in Figs. 9(c) and 10(c). This corresponds well to the conclusions drawn in [35] regarding the residual stiffness changes in repeated longitudinal compression tests.

The concept of "elapsed time" in Fig. 6 is further adopted here for the CFR tests. The strain–time curves for each loading-fatigue-recovery interval are shifted to the origin for better comparison. The results are shown in Figs. 11 and 12. The solid blue curves indicate the first loading for each applied SL, whereas the red dashed curves depict the second loading at the same SL.

Figs. 11 and 12 confirm the much lower strain accumulation across all CFR tests than that in CCR tests. For both 0.1 Hz and 1 Hz, the

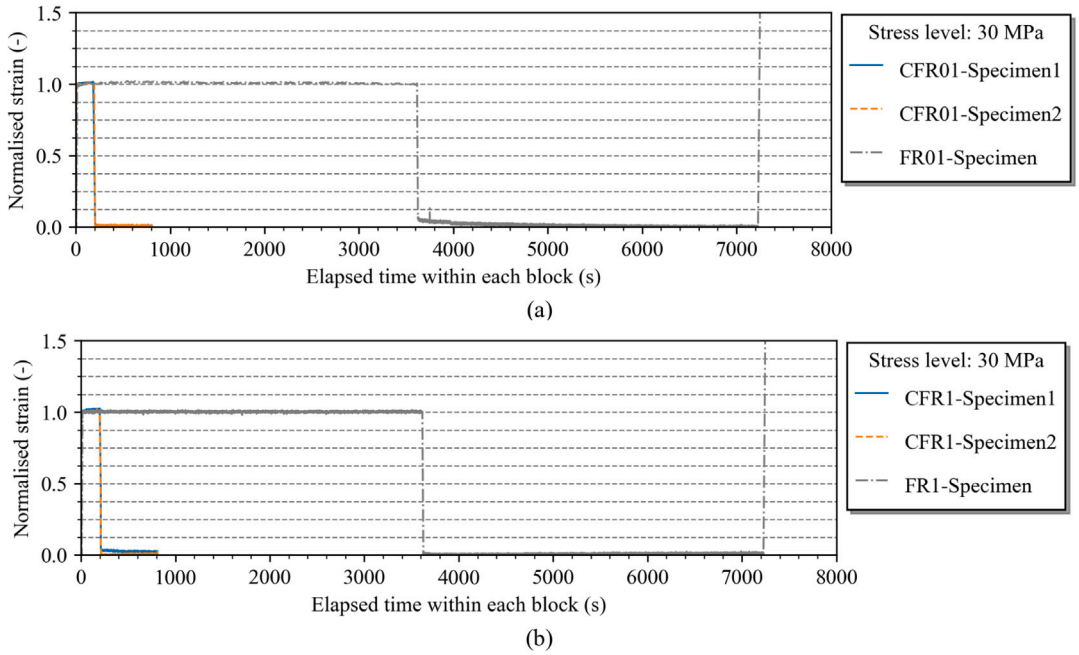


Fig. 13. Comparison between fatigue-recovery (FR) and cyclic fatigue-recovery (CFR) tests at the same stress level: (a) at a loading frequency of 0.1 Hz; (b) at a loading frequency of 1 Hz.

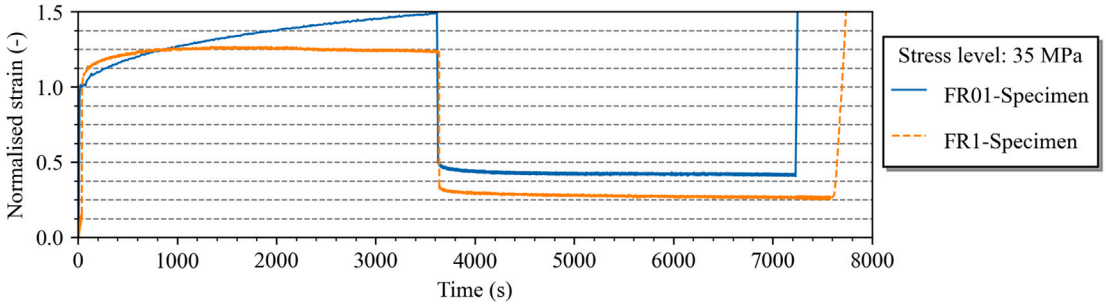


Fig. 14. Fatigue-recovery (FR) of different loading frequencies at a relatively high stress level.

strain accumulation up to 25 MPa remains negligible. At 30 MPa, there is observable strain accumulation, but no marked difference can be found between the two frequencies. Furthermore, at both frequencies, no significant difference is observed between the 1st (blue) and 2nd (red) loading for the same SL. Thus, it can be inferred that no clear viscoplastic strain develops under the tested conditions. This suggests that the nonlinearity threshold in the CFR tests is substantially higher than in the CCR tests, likely exceeding 30 MPa, despite both being conducted with the same load duration of 200 s.

A previous study [35] also applied the same loading–fatigue–recovery sequence (fatigue loading for 200 s and recovery for 600 s). The examined material was the same species but with a higher density, ranging from 580 to 620 kg/m^3, compared to 495–510 kg/m^3 in this work. Instead of stepwise-increasing SL as in this study, a fixed SL of 78% was applied to all specimens at 1 Hz, and the sequence was repeated five and ten times, respectively. There, a much clearer strain accumulation was observed, in contrast to the 30-MPa interval (75% SL) in this study. Apart from that, analysis of the differences between consecutive loading sequences (see Fig. 7 in [35]) indicated that the first loading sequence exhibited a higher accumulation rate than the subsequent ones, which is likely attributable to viscoplastic strain development during the first loading interval at that stress level.

The test machine and strain-measurement technique used in both studies are identical; however, in [35], the climate conditions during fatigue loading were not strictly controlled (an average moisture content loss of 0.3% was observed). Therefore, one possibility is that the absence of constant climate control in the previous study might have promoted strain accumulation through a mechanism analogous to the mechanosorptive creep.

3.1.5. Fatigue recovery test (FR)

Due to the limited amount of accumulated strain observed in CFR tests, only the highest SL (30 MPa) is selected for implementation in the FR test, with a loading duration of one hour. The normalized results are shown in Fig. 13. The specimens tested at 0.1 Hz and 1 Hz are both characterized by a residual strength of 38.4 MPa. The specimens tested at both frequencies show negligible strain accumulation and recovery, despite the extended test duration.

The results from the additional group with an even higher SL of 35 MPa are illustrated in Fig. 14. The tested specimens have residual strengths of 40.1 MPa and 40.9 MPa at test frequencies of 0.1 Hz and 1 Hz, respectively. The distinction between the two test frequencies becomes clear, with a much more pronounced development of the viscoplastic strain component in the 0.1 Hz group (higher residual strain at the end of the recovery phase). This observation is consistent with the trend reported in [35], where fatigue loading at 0.1 Hz at the same stress level resulted in greater strain accumulation than loading at 1 Hz for the same duration.

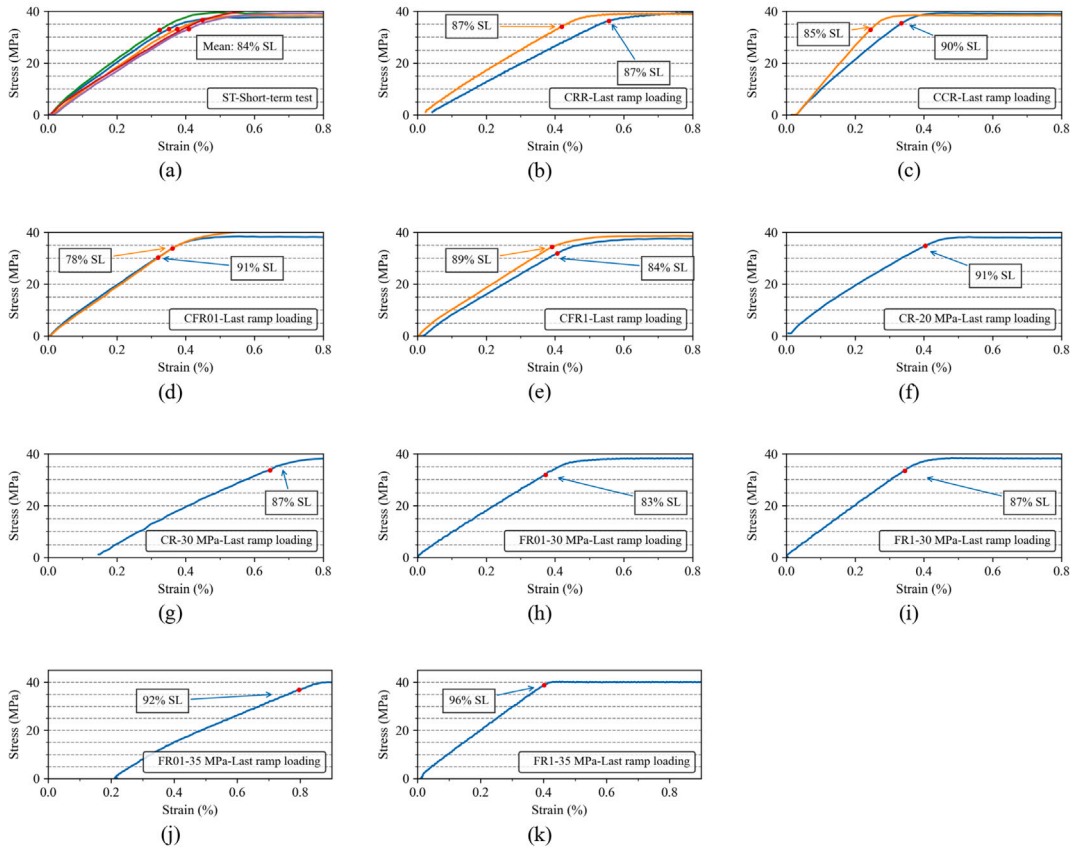


Fig. 15. Proportional limit obtained from: (a) short-term loading test; (b) the last ramp loading of cyclic ramp-recovery (CRR) tests; (c) the last ramp loading of cyclic creep-recovery (CCR) tests; (d) the last ramp loading of cyclic fatigue-recovery tests at 0.1 Hz (CFR01); (e) the last ramp loading of cyclic fatigue-recovery tests at 1 Hz (CFR1); (f) the last ramp loading of creep-recovery (CR) tests at 20 MPa; (g) the last ramp loading of creep-recovery (CR) tests at 30 MPa; (h) the last ramp loading of fatigue-recovery tests at 0.1 Hz (FR01) at 30 MPa; (i) the last ramp loading of fatigue-recovery tests at 1 Hz (FR1) at 30 MPa; (j) the last ramp loading of fatigue-recovery tests at 0.1 Hz (FR01) at 35 MPa; (k) the last ramp loading of fatigue-recovery tests at 1 Hz (FR1) at 35 MPa.

3.2. Proportional limit analysis

The stress–strain curves from residual strength tests of all test groups are compiled in Fig. 15 to enable a systematic analysis of the 'apparent' proportional limit. The determined proportional limits predominantly lie above 80%. This corresponds to the values reported in [20], indicating that the European ash used in this work likely has a high proportional limit under compression parallel to the grain. Besides the relatively high proportional limit, the hardening behavior after entering the plastic zone appears much sharper than the predicted curves presented in [31].

The short-term tested specimens exhibit an average proportional limit of 84.2 ± 2.2%, which is at the lower bound among other test groups (87.6 ± 4.4%). This higher 'apparent' proportional limit maybe associated with the loading history of the other test groups. Given the adopted viscoplasticity formulation, prior loading above nonlinearity onset results in accumulated viscoplastic strain and the associated evolution of hardening variable. In subsequent loading, additional viscoplastic deformation may occur at a higher stress level. From a physical perspective, this behavior may be attributed to the irreversible microstructural rearrangement and local consolidation during prior loading. At the cell wall level, this may be interpreted as cellulose microfibrils sliding and rearranging, forming new intermolecular bonds that increase the resistance to further deformation. This phenomenon is most evident in the two fatigue groups tested at 35 MPa for 1 h. The identified proportional limit in the 0.1 Hz and 1 Hz group reaches 92% and 96%, respectively.

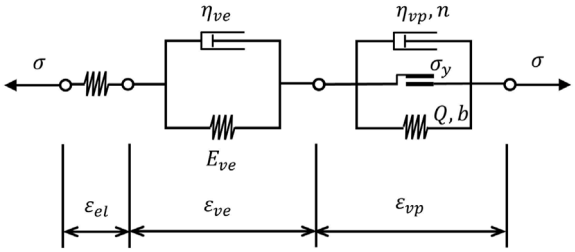


Fig. 16. Theoretical coupled elasto–viscoelastic–viscoplastic model for European Ash under compression parallel-to-grain.

4. Theoretical analysis

4.1. Coupled elasto–viscoelastic–viscoplastic model

A phenomenological model comprising an elastic spring, a Kelvin–Voigt viscoelastic branch, and a Perzyna-type viscoplastic branch with isotropic hardening was thus proposed to describe the observed strain response of European Ash under longitudinal compression, as illustrated in Fig. 16.

For problems undergoing infinitesimal strains, the additive decomposition of the total strain tensor applies, as denoted in Eq. (1). The elastic strain tensor $\boldsymbol{\varepsilon}^{e}$ and viscoelastic strain tensor $\boldsymbol{\varepsilon}^{ve}$ account for instantaneous and time-dependent reversible deformation, respectively. Whereas the viscoplastic part $\boldsymbol{\varepsilon}^{vp}$ captures irreversible deformation

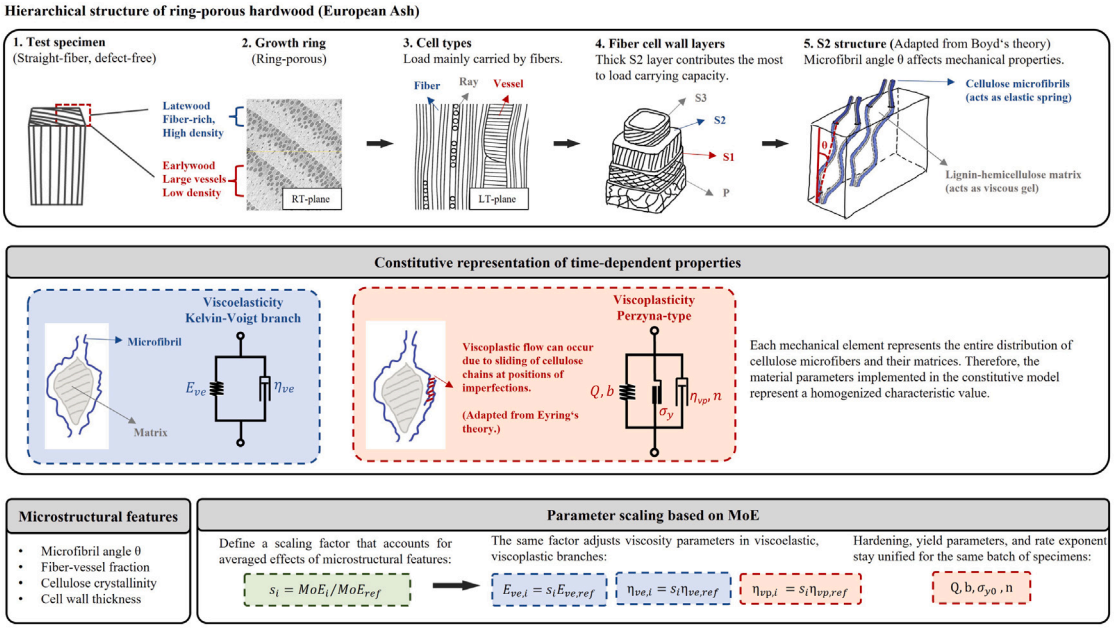


Fig. 17. From hierarchical structure to coupled elasto–viscoelastic–viscoplastic constitutive model: microstructural interpretation of MoE-based viscoelastic and viscoplastic parameter scaling in European Ash. Microstructural model adapted from Boyd's theory [39] and Eyring's theory [40].

under sustained or cyclic loading.

$$\boldsymbol{\varepsilon} = \boldsymbol{\varepsilon}^{\mathrm{e}} + \boldsymbol{\varepsilon}^{\mathrm{ve}} + \boldsymbol{\varepsilon}^{\mathrm{vp}} \tag{1}$$

Under constant environmental conditions, the thermodynamic free energy potential can be decoupled in an additive manner in the following form:

$$\begin{aligned}\psi &= \psi^{e}(\boldsymbol{\varepsilon}^{\mathrm{e}}) + \psi^{\mathrm{ve}}(\boldsymbol{\varepsilon}^{\mathrm{ve}}) + \psi^{\mathrm{vp}}(r) \\ &= \psi^{e}(\boldsymbol{\varepsilon} - \boldsymbol{\varepsilon}^{\mathrm{ve}} - \boldsymbol{\varepsilon}^{\mathrm{vp}}) + \psi^{\mathrm{ve}}(\boldsymbol{\varepsilon}^{\mathrm{ve}}) + \psi^{\mathrm{vp}}(r)\end{aligned} \tag{2}$$

where ψ^{e} and ψ^{ve} indicate the energy stored in the elastic and viscoelastic component, respectively; ψ^{vp} represents the stored energy associated with isotropic hardening. The viscoplastic flow is purely dissipative. The scalar variable r describes the accumulated plastic strain that governs isotropic hardening.

In this work, uniaxial compression tests conducted along a single loading direction were taken into account. Accordingly, the proposed constitutive model can be formulated in its 1D form. However, it is noted that wood exhibits strong anisotropy, and in general, a three-dimensional constitutive formulation is required to predict the nonlinear mechanical behavior of structural timber elements. The extension to general 3D formulation would require at least the following adaptations: definition of direction-dependent stiffnesses and viscosities, formulation of anisotropic or orthotropic yield surfaces and hardening laws (i.e., those used in [31,41]), and distinction between different loading modes—for instance, accounting for potentially limited viscoplasticity development under tension or shear.

The Cauchy stress can be derived from the free energy, which follows the generalized Hooke's law:

$$\sigma = \frac{\partial \psi}{\partial \varepsilon} = E\left(\varepsilon - \varepsilon^{ve} - \varepsilon^{vp}\right) \tag{3}$$

where E denotes the modulus of elasticity in the longitudinal direction of the material.

The generalized Kelvin–Voigt model has been widely adopted to describe the viscoelastic strain in wood [32,42,43]. Due to the relatively short loading duration in this work, a single branch Kelvin–Voigt model was used. The viscoelastic strain evolves according to:

$$\dot{\varepsilon}^{ve} = \frac{1}{\eta_{ve}}\left(\sigma - E_{ve}\varepsilon^{ve}\right) \tag{4}$$

where E_{ve} denotes the viscoelastic modulus; η_{ve} is the viscosity in the viscoelastic term, which fulfills the following relationship with retardation time: $\eta_{ve} = E_{ve}\,\tau_{ve}$.

The yield function is defined with the Voce hardening law according to [41] as:

$$f(\sigma, r) = |\sigma| - \sigma_y(r) \tag{5}$$

$$\sigma_y(r) = \sigma_{y0} + Q\left(1 - e^{-br}\right) \tag{6}$$

where σ_{y0} denotes the initial yield stress; Q and b are the isotropic hardening parameters that control saturation.

The viscoplastic strain rate $\dot{\varepsilon}^{vp}$ is expressed based on the associated flow rule as [44]:

$$\dot{\varepsilon}^{vp} = \dot{r}\,\mathrm{sign}(\sigma) \tag{7}$$

The equivalent viscoplastic strain rate follows classical Perzyna-type formulation [45] and evolves through Norton's power law [46] as:

$$\dot{r} = \left\langle \frac{f(\sigma, r)}{\eta_{vp}} \right\rangle^{n} \tag{8}$$

where η_{vp} and n denote the viscosity parameter and the rate exponent that control rate sensitivity, respectively; $\langle\cdot\rangle$ denotes the Macaulay brackets: $\langle x\rangle = \max(x, 0)$.

Substituting Eq. (8) into Eq. (7), the viscoplastic strain evolution can be computed:

$$\dot{\varepsilon}^{vp} = \left\langle \frac{f(\sigma, r)}{\eta_{vp}} \right\rangle^{n} \mathrm{sign}(\sigma) \tag{9}$$

4.2. Calibration using multi-specimen creep data

The presented 1D constitutive model characterizes a total of eight material parameters to be identified, including the reference MoE, the reference viscoelastic modulus $E_{ve,ref}$, the reference viscoelastic viscosity $\eta_{ve,ref}$, the reference viscoplastic viscosity parameter $\eta_{vp,ref}$, the common viscoplastic rate exponent n, the common yield strength σ_{y0}, and the common hardening parameters b, Q (see Table 2). Among those parameters, the MoE is relatively easy to identify. As illustrated in Section 3, for multi-stress-level test groups (CRR, CCR and CFR), the

MoE can be obtained by computing the net strain increase during the first loading of each load sequence. Whereas for the single-stress-level groups (CR and FR), the MoE can be estimated using the initial elastic strain at the intended stress level.

The remaining material parameters reflect the coupled effects of material nonlinearity and time-dependency and thus cannot be calibrated using a single test group. Since the measured MoE varied considerably across specimens, the magnitude of the time-dependent strain response is expected to vary accordingly. Consequently, a calibration framework is required to account for specimen-to-specimen variability while enabling the identification of a common set of constitutive parameters across multiple test series. The following presents key assumptions underlying the proposed MoE-based parameter scaling approach. A visualization is illustrated in Fig. 17.

- The measured MoE is assumed to reflect specimen-to-specimen variations arising from microstructural features which are difficult to measure macroscopically, such as microfibril angle, fiber-vessel fraction, cellulose crystallinity, and cell wall thickness.
- Following Boyd's interpretation of viscoelastic behaviors of wood [39], cellulose microfibrils act as load-bearing elastic springs, whereas the surrounding lignin–hemicellulose matrix can be perceived as a viscous gel. Therefore, the same microstructural features are expected to affect time-dependent mechanical responses in a similar manner. Here, a simplified proportional scaling relationship was assumed. The viscoelastic modulus $E_{\mathrm{ve,i}}$ and viscosity $\eta_{\mathrm{ve,i}}$ of each specimen were obtained by scaling a common reference value, MoE_{ref}, according to each specimen's own MoE. Similarly, the viscosity parameter $\eta_{vp,i}$ in the viscoplastic branch was scaled. The viscoplastic deformation is assumed to originate from cellulose chain sliding within the microfibrils at locations of imperfections (adapted from Eyring's deformation kinetics theory of polymers [40]). In contrast, a common set of yield and hardening parameters was assumed for all specimens. This is supported by previous analysis of the proportional limit in Section 3.2, which indicated comparably low variability (87.6 ± 4.4%). Furthermore, the rate exponent n was also treated as a material constant, as variations in n strongly affect the flow rate and could dominate the calibration.

To accurately identify these remaining parameters, the calibration dataset must provide sufficient time-dependent strain accumulation and reflect strain evolution across different stress levels and time scales. As a result, the following test groups, CCR, CR20 and CR30, were used for parameter identification.

The calibration framework was developed in Python to perform inverse parameter identification of the constitutive model. The numerical model was integrated using an implicit Backward Euler scheme. NumPy and Pandas were employed for numerical computation and data handling, while parameter optimization was carried out using the trust-region reflective algorithm implemented in 'scipy.optimize.least_squares', minimizing the residual between the simulated and experimentally measured strain histories under stress-controlled loading.

The calibrated reference parameters, common parameters, and the specimen-specific MoE used for scaling are presented in Table 2. The calibrated numerical model achieved good agreement with experimental observations under both short- and long-period creep loadings. Especially for the longer-period creep tests, the material response at both the holding phase and the recovery phase was successfully reproduced. The comparison between the experimental results and the simulation is shown in Fig. 18.

Despite the relatively good fit, the identified constitutive parameters should not be interpreted as the only set that sufficiently describes the observed material behavior. In this work, a total of seven unknown parameters were calibrated on datasets with a relatively rich stress history that includes loading, unloading, recovery, sustained loading at two time scales, and multiple stress levels. Nevertheless, different parameter combinations may still reproduce similar strain responses. Further experiments are needed to enable a systematic analysis of parameter sensitivity, identifiability, and uncertainty quantification.

Table 2
Identified material parameters in the proposed constitutive model.

Common parameters			Scaling	
Parameter	Unit	Value	Specimen	MoE [GPa]
MoE_{ref}	[GPa]	11	CCR-1	11.7
$E_{\mathrm{ve,ref}}$	[GPa]	160	CCR-2	14.9
$\eta_{\mathrm{ve,ref}}$	[GPa s]	31 000	CR20	9.7
$\eta_{\mathrm{vp,ref}}$	[GPa s]	27 000	CR30	6.8
n	[–]	1.014	FR135	8.0
σ_{y0}	[MPa]	19	FR0135	6.7
b	[–]	250	FR130	9.7
Q	[MPa]	18	FR0130	8.6

The general applicability of the proposed model beyond the investigated test conditions requires further investigation. For instance, compression perpendicular to the grain in wood is known to exhibit pronounced delayed deformation associated with the viscous lignin–hemicellulose matrix. In contrast, different deformation and failure mechanisms may govern tensile and shear loading, essentially changing the nonlinearity threshold. For other wood species (potentially also for certain engineered wood product types), the proposed framework may remain applicable to compression along the dominant fiber direction. However, the calibrated model parameters in this work should not be considered representative of other materials. Under varying moisture or temperature conditions, besides formulating model parameters such as stiffness as climate-dependent, additional deformation mechanisms, especially mechanosorption, need to be incorporated to account for the interaction between mechanical loading and climate conditions.

4.3. Applicability of calibrated model to cyclic loading

To assess the calibrated model's transferability to fatigue loading, simulations were performed under four cyclic loading conditions: two loading frequencies (0.1 Hz and 1 Hz) and two stress levels (30 MPa and 35 MPa). The previously calibrated model parameters were used, scaled based on the MoE of individual specimens. Figs. 19 and 20 visualize the comparison between the simulated and experimental responses for 30 MPa and 35 MPa, respectively. To provide a detailed analysis of the strain decomposition predicted by the model, the envelopes of predicted individual strain components are also shown in the same figure.

At 30 MPa, the experimental strain envelope remains nearly horizontal for both test frequencies, whereas the model predicts clear strain accumulation for both frequencies. Decomposition of the simulated response indicates that this discrepancy mainly results from the Perzyna viscoplastic strain component. Considering that the model was calibrated against both 200-second and one-hour creep tests at the same stress level and that the strain development was reasonably well reproduced, it is unlikely that the discrepancy observed here can be explained solely by inadequate calibration. Instead, it may indicate a limitation of the current viscoplastic formulation in sufficiently capturing material response under cyclic loading.

In the current model, the viscoplastic flow rate is governed by the Perzyna overstress formulation, while the evolution of viscoplastic resistance is described by Voce isotropic hardening. During cyclic loading, viscoplastic strain accumulates whenever the applied stress exceeds the evolving viscoplastic threshold. Due to the repeated reduction in stress during each cycle, the model predicts substantially less viscoplastic strain accumulation than under sustained loading at the same maximum stress. However, additional mechanisms associated with cyclic stabilization, for instance, cannot be captured by the model.

At the higher stress level of 35 MPa, a different discrepancy is observed: the experimental results exceed the numerical prediction,

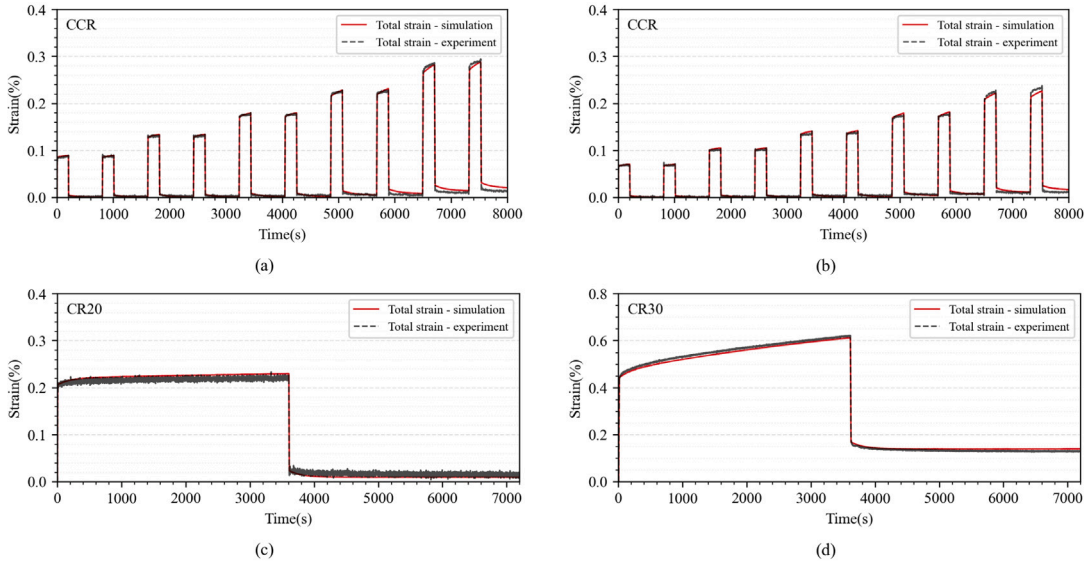


Fig. 18. Comparison between experiment results and simulation results for the calibration dataset: (a) specimen 1 from CCR (cyclic-creep-recovery) test series; (b) specimen 2 from CCR test series; (c) CR20 (creep-recovery test at 20 MPa); (d) CR30 (creep-recovery test at 30 MPa).

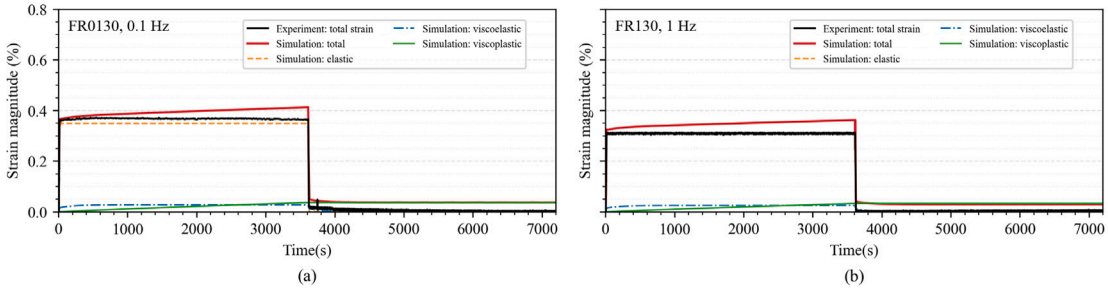


Fig. 19. Comparison between experiment results and simulation results for the validation dataset: (a) FR0130 (fatigue-recovery test at a maximum stress of 30 MPa, test frequency of 0.1 Hz); (b) FR130 (fatigue-recovery test at a maximum stress of 30 MPa, test frequency of 1.0 Hz).

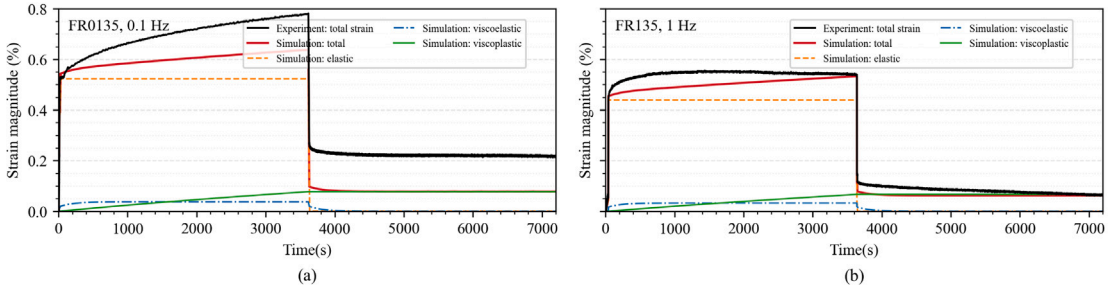


Fig. 20. Comparison between experiment results and simulation results for the validation dataset: (a) FR0135 (fatigue-recovery test at a maximum stress of 35 MPa, test frequency of 0.1 Hz); (b) FR135 (fatigue-recovery test at a maximum stress of 35 MPa, test frequency of 1.0 Hz).

especially in the lower-frequency case. Examination of cyclic stiffness during loading reveals a progressive decrease in both specimens, although to varying degrees. As a result, the previous assumption that prior loading history does not affect material properties is no longer valid for stress levels as high as 35 MPa (roughly 87% of the mean short-term strength). Damage or other degradation mechanisms, which are not represented in the current constitutive formulation, therefore likely contribute to the underprediction of deformation. Coupling the current viscoelastic–viscoplastic formulation with an appropriate damage description should consequently be considered for the high-stress regime.

However, the discrepancy at 35 MPa cannot be explained solely by progressive material degradation. This is particularly evident for the 1 Hz specimen. The experimentally obtained strain initially increases at a much higher rate than the numerical prediction. This is consistent with the previous observation that additional damage-related mechanisms are not captured by the current model. At around 1500s, however, the strain accumulation approaches a plateau, followed by a slight decrease in strain, causing the prediction and the test result to converge at the end of one-hour cyclic loading. This indicates that multiple competing mechanisms may govern the response under cyclic loading at high stress levels: material degradation may promote accelerated strain accumulation, whereas other cyclic and/or frequency-dependent mechanisms seem to suppress or partially reverse strain accumulation. An additional explanation may be the hysteresis-induced self-heating, which can substantially alter material

properties [30]. Although the surface temperature of test specimens was not measured in the current work, Clorius [36] reported a surface temperature rise of 2–3 degrees within an hour of compressive fatigue tests at 1 Hz. Further investigation is required before the observed discrepancies can be attributed to specific mechanisms.

5. Conclusion and outlook

In this work, a relatively short-duration testing campaign suitable for nonlinearity characterization of wood in longitudinal compression was developed. The complete test plan covers ramp, creep, and fatigue loading at different frequencies. By applying load-recovery sequences of different stress levels to the same specimen, the influence of sample-to-sample variability on the results was minimized, enabling to draw the following conclusions using a small number of tests:

- The ramp, creep, and fatigue tests exhibit qualitatively similar strain responses, consisting of elastic, viscoelastic, and viscoplastic components. Notably, even ramp loading at a relatively low stress rate (3 MPa/s) produces measurable viscoelastic and viscoplastic strain accumulation.
- At the same stress level, creep loading seems to induce much higher strain accumulation over time compared to fatigue loading of the same duration. When the applied stress is sufficiently high, the lower test frequency of 0.1 Hz appears to yield a higher strain response than the 1 Hz group.
- Compared to classical rate-independent plasticity, viscoplasticity theory provides a more coherent explanation for the observed unrecovered strain responses across different loading types. The nonlinearity threshold — above which permanent time-dependent strain accumulation develops — depends strongly on both loading type and duration. For the investigated cyclic ramp tests, this threshold lies between 75% and 88% of the average ultimate strength. However, the threshold decreases to 50% and 62.5% for the 200-second creep tests. Fatigue tests with the same maximum stress and the same duration appear to have a much higher threshold than in the creep tests.

These findings confirm the relevance of a viscoplasticity-based framework for design-oriented modeling of nonlinear deformation of wood in longitudinal compression. Accordingly, a one-dimensional constitutive model consisting of a Kelvin–Voigt viscoelastic branch and a Perzyna-type viscoplastic branch was proposed. To account for specimen-to-specimen variability, the experimentally measured Modulus of Elasticity (MoE) for each specimen was treated as a macroscopic descriptor of its underlying microstructural variation and used to scale the viscoelastic and viscoplastic viscosity parameters. In contrast, the hardening and rate-sensitivity parameters were calibrated globally and assumed to remain consistent within the given batch of wood with similar macroscopic characteristics (density).

The resulting MoE-based calibration framework achieved consistent agreement across multiple specimens and different creep loading paths, indicating that a substantial portion of the observed scattering can be attributed to microstructure-dependent stiffness variations. Finally, the same constitutive model, together with the identified material parameters, was applied to fatigue loading to assess its applicability to cyclic loading. At 30 MPa, the model overestimated the progressive accumulation of viscoplastic strain, whereas at 35 MPa, the experimental response exhibited progressive stiffness degradation that the present uncoupled VE–VP formulation cannot capture. Furthermore, the experimental results at 35 MPa and 1 Hz showed a non-monotonic evolution of the maximum strain envelope, characterized by a high initial strain accumulation rate, subsequent strain stabilization, and a slight decrease towards the end of loading. The adopted rate-dependent Perzyna formulation with Voce isotropic hardening captured the significantly lower strain response under cyclic loading than under sustained loading at the same maximum stress. However, it cannot account for the complex interacting mechanisms under cyclic loading, such as cyclic stabilization or frequency dependence.

Future work should therefore focus on more detailed cyclic experiments to characterize these additional mechanisms. Analysis of cyclic stiffness and hysteresis, and potential monitoring of the specimen's surface temperature, are needed to identify a more suitable modeling framework for cyclic loading. In particular, the progressive stiffness degradation at high stress levels indicates the need to investigate coupling between viscoplasticity and damage. Furthermore, a larger number of replicates per group is required for statistical analysis to account for the high variability in specimen properties and to draw more general conclusions regarding the time-dependent nonlinear behavior of the investigated material under compression.

CRediT authorship contribution statement

Changxi Yang: Writing – review & editing, Writing – original draft, Methodology, Investigation, Formal analysis, Conceptualization. **Mostafa Abdelrahman:** Writing – review & editing, Methodology, Investigation, Conceptualization. **Ani Khaloian-Sarnaghi:** Writing – review & editing, Supervision, Methodology, Funding acquisition, Conceptualization. **Yaman Dalal:** Methodology, Formal analysis. **Jan-Willem van de Kuilen:** Writing – review & editing, Supervision, Methodology, Funding acquisition, Conceptualization.

Declaration of competing interest

The authors declare that they have no known competing financial interests or personal relationships that could have appeared to influence the work reported in this paper.

Acknowledgments

This study was partially funded by the German Federal Ministry of Food and Agriculture through the Fachagentur Nachwachsende Rohstoffe e.V. (FNR) (grant number 22009817, HS-Hybrid project). The authors gratefully acknowledge the support of the Bavarian State Ministry of Food, Agriculture and Forestry in the WoodVibes project (grant number: LWF-A9-7831-26-4-1).

Data availability

The authors do not have permission to share data.

References

[1] F.F.P. Kollmann, W.A. Côté, Principles of Wood Science and Technology: I Solid Wood, Springer Berlin Heidelberg, Berlin, Heidelberg, 1968, http://dx.doi.org/10.1007/978-3-642-87928-9.

[2] P.U.A. Grossman, M.B. Wold, Compression fracture of wood parallel to the grain, Wood Sci. Technol. 5 (2) (1971) 147–156, http://dx.doi.org/10.1007/BF01134225.

[3] M. Bariska, L.J. Kuera, On the fracture morphology in wood: Part 2: Macroscopical deformations upon ultimate axial compression in wood, Wood Sci. Technol. 19 (1985) 19–34.

[4] A. Reiterer, S.E. Stanzl-Tschegg, Compressive behaviour of softwood under uniaxial loading at di erent orientations to the grain, Mech. Mater. 33 (2001) 705–715.

[5] S. Ellis, P. Steiner, The behaviour of five wood species in compression, IAWA J. 23 (2) (2002) 201–211, http://dx.doi.org/10.1163/22941932-90000298.

[6] M. Brabec, J. Tippner, V. Sebera, J. Milch, P. Rademacher, Standard and non-standard deformation behaviour of European beech and Norway spruce during compression, Holzforschung 69 (9) (2015) 1107–1116, http://dx.doi.org/10.1515/hf-2014-0231.

[7] J.M. Dinwoodie, Failure in timber part II: The angle of shear through the cell wall during longitudinal compression stressing, Wood Sci. Technol. 8 (1) (1974) 56–67, http://dx.doi.org/10.1007/BF00350643.

[8] L.J. Kučera, M. Bariska, On the fracture morphology in wood: Part 1: A SEM-study of deformations in wood of spruce and aspen upon ultimate axial compression load, Wood Sci. Technol. 16 (4) (1982) 241–259, http://dx.doi.org/10.1007/BF00353147.
[9] M. Gong, Failure of Spruce Under Compressive Low-Cycle Fatigue Loading Parallel to Grain (Ph.D. thesis), The University of New Brunswick, Canada, 2002.
[10] H. Tresca, Notes sur l'écoulement des corps solides soumis à de fortes pressions, Comptes Rendus de L'Académie Des Sci. 59 (1864) 754–758.
[11] R. von Mises, Mechanik der festen Körper im plastisch deformablen Zustand, Nachrichten Von der Ges. der Wiss. Zu Gött. Math.-Physikalische Kl. (1913) 582–592.
[12] R. Hill, The Mathematical Theory of Plasticity, Clarendon Press, Oxford, UK, 1950.
[13] J.C. Maxwell, The Scientific Papers of James Clerk Maxwell, vol. 2, Cambridge University Press, Cambridge, UK, 1890.
[14] W. Thomson, Mathematical and Physical Papers, vol. 1, Cambridge University Press, Cambridge, UK, 1890.
[15] W. Robinson, The microscopic features of mechanical strains in timber and the bearing of these on the structure of the cell wall in plants, Philos. Trans. R. Soc. Lond. Ser. B, Contain. Pap. A Biol. Character 210 (1920) 48–82.
[16] J. Kisser, A. Steininger, Makroskopische und mikroskopische Strukturänderungen bei der Biegebeanspruchung von Holz, Holz Als Roh- Und Werkst. 10 (11) (1952) 415–421.
[17] J.M. Dinwoodie, Failure in timber. Part I. Microscopic changes in cell-wall structure associated with compression failure, J. Inst. Wood Sci. 21 (1968) 37–53.
[18] R.S.T. Kingston, B. Budgen, Some aspects of the rheological behaviour of wood part IV: Non-linear behaviour at high stresses in bending and compression, Wood Sci. Technol. 6 (3) (1972) 230–238, http://dx.doi.org/10.1007/BF00351580.
[19] E. Bolza, N.H. Kloot, The Mechanical Properties of 174 Australian Timbers, Technical Paper 25, Division of Forest Products, C.S.I.R.O., Australia, 1963.
[20] Verbundvorhaben: Holzbasierte Werkstoffe im Maschinenbau (HoMaba), Berechnungskonzepte, kennwertanforderungen, kennwertermittlung, 2022, Research project, Unpublished project results.
[21] C. Keith, The mechanical behaviour of wood in longitudinal compression, Wood Sci. 4 (4) (1972) 234–244.
[22] R.S.T. Kingston, L.N. Clarke, Some aspects of the rheological behaviour of wood. I. The effect of stress with particular reference to creep. II. Analysis of creep data by reaction-rate and thermodynamic methods, Aust. J. Appl. Sci. 12 (1961) 211–249, Cited in Kingston and Budgen, 1972.
[23] P.U.A. Grossman, Research on the rheology of wood, Holzforschung 17 (5) (1963) 146–149, http://dx.doi.org/10.1515/hfsg.1963.17.5.146.
[24] L. Bach, Non-Linear Mechanical Behavior of Wood in Longitudinal Tension (Ph.D. thesis), College of Forestry at Syracuse University, Michigan, 1966.
[25] D.G. Hunt, Linearity and non-linearity in mechano-sorptive creep of softwood in compression and bending, Wood Sci. Technol. 23 (4) (1989) 323–333, http://dx.doi.org/10.1007/BF00353248.
[26] H. Kuwamura, Creep limit of wood under parallel-to-grain compression, J. Struct. Constr. Eng. (Trans. AIJ) 77 (681) (2012) 1691–1700, http://dx.doi.org/10.3130/aijs.77.1691.
[27] K. Hayashi, B. Felix, C. Le Govic, Wood viscoelastic compliance determination with special attention to measurement problems, Mater. Struct. 26 (6) (1993) 370–376, http://dx.doi.org/10.1007/BF02472963.
[28] Z. Cai, K.J. Fridley, Creep and creep-recovery models for wood under high stress levels, Wood Fiber Sci. 34 (3) (2002) 425–433.
[29] L. Bach, Frequency-dependent fracture in wood under pulsating loading, 1975.
[30] C. Yang, M. Abdelrahman, A. Khaloian-Sarnaghi, J.-W. Van De Kuilen, A comprehensive analysis of fatigue in wood and wood products, Int. J. Fatigue 194 (2025) 108807, http://dx.doi.org/10.1016/j.ijfatigue.2025.108807.
[31] M. Wang, X. Song, X. Gu, Three-dimensional combined elastic-plastic and damage model for nonlinear analysis of wood, J. Struct. Eng. 144 (8) (2018) 04018103, http://dx.doi.org/10.1061/(ASCE)ST.1943-541X.0002098.
[32] S. Fortino, F. Mirianon, T. Toratti, A 3D moisture-stress FEM analysis for time dependent problems in timber structures, Mech. Time-Depend. Mater. 13 (4) (2009) 333–356, http://dx.doi.org/10.1007/s11043-009-9103-z.
[33] P. Perzyna, The constitutive equations for rate sensitive plastic materials, Quart. Appl. Math. 20 (4) (1963) 321–332.
[34] E.A. de Souza Neto, D. Perić, D.R.J. Owen, Computational Methods for Plasticity: Theory and Applications, first ed., Wiley, 2008, http://dx.doi.org/10.1002/9780470694626.
[35] M. Abdelrahman, C. Yang, A. Khaloian, K. Achterhold, F. Pfeiffer, J.-W. van de Kuilen, Influence of frequency and recovery interval on fatigue behavior of wood in compression, Holzforschung 80 (2) (2026) 99–114, http://dx.doi.org/10.1515/hf-2025-0104.
[36] C.O. Clorius, M.U. Pedersen, P. Hoffmeyer, L. Damkilde, Compressive fatigue in wood, Wood Sci. Technol. 34 (1) (2000) 21–37, http://dx.doi.org/10.1007/s002260050005.
[37] Z. Yang, H. Wei, V. Borghese, M. Zucca, F. Stochino, Y. Xiao, C. Demartino, Long-term creep behaviour of cross-laminated bamboo and timber under axial compression: Experimental and probabilistic modelling, Constr. Build. Mater. 515 (2026) 145470, http://dx.doi.org/10.1016/j.conbuildmat.2026.145470.
[38] A.P. Schniewind, Recent progress in the study of the rheology of wood, Wood Sci. Technol. 2 (3) (1968) 188–206, http://dx.doi.org/10.1007/BF00350908.
[39] J.D. Boyd, An anatomical explanation for visco-elastic and mechano-sorptive creep in wood, and effects of loading rate on strength, in: P. Baas (Ed.), New Perspectives in Wood Anatomy, Vol. 1, Springer Netherlands, 1982, pp. 171–222.
[40] A.S. Krausz, H. Eyring, Deformation Kinetics, John Wiley & Sons, New York, 1975.
[41] F. Seeber, A. Khaloian-Sarnaghi, T. Yu, F. Duddeck, J.-W. Van De Kuilen, Development and validation of an orthotropic 3D elasto-plastic damage model for wood, considering fiber deviations, Eng. Struct. 308 (2024) 117928, http://dx.doi.org/10.1016/j.engstruct.2024.117928.
[42] M.M. Hassani, F.K. Wittel, S. Hering, H.J. Herrmann, Rheological model for wood, Comput. Methods Appl. Mech. Engrg. 283 (2015) 1032–1060, http://dx.doi.org/10.1016/j.cma.2014.10.031.
[43] T. Yu, A. Khaloian, J.-W. van de Kuilen, An improved model for the time-dependent material response of wood under mechanical loading and varying humidity conditions, Eng. Struct. 259 (2022) 114116, http://dx.doi.org/10.1016/j.engstruct.2022.114116.
[44] J.C. Simo, T.J.R. Hughes, Computational Inelasticity, in: Interdisciplinary Applied Mathematics, vol. 7, Springer-Verlag, New York, 1998, http://dx.doi.org/10.1007/b98904.
[45] P. Perzyna, Fundamental problems in viscoplasticity, in: Advances in Applied Mechanics, Vol. 9, Elsevier, 1966, pp. 243–377, http://dx.doi.org/10.1016/S0065-2156(08)70009-7.
[46] J. Lemaitre, J.-L. Chaboche, B. Shrivastava, J. Lemaitre, Mechanics of Solid Materials, first ed., Cambridge Univ. Press, Cambridge, 2002, paperback ed., repr., transferred to digital print.